Supplemental Material

Video captions

Video S1. Growth of attached *S. aureus* (green) in a control experiment without added neutrophils (4 h).

Video S2. *S. aureus* biofilm growth visualized by brightfield microscopy from time t = 0.5 to 8 hours in 10% serum. This is the same field of view as Video S3.

Video S3. *S. aureus* biofilm growth visualized by overlaid brightfield and fluorescence microscopy from time t = 0.5 to 8 hours in 10% serum. Green fluorescence consistently overlaps all bacterial biomass (Video S2) indicating retention of the GFP-encoding plasmid.

Video S4. Interaction of neutrophils (red) with attached *S. aureus* (green) at an intermediate neutrophil density of ~3000 per cm^{-2} and N:B ratio of 0.24 (4 h).

Video S5. Interaction of neutrophils (red) with attached *S. aureus* (green) at a high neutrophil density of ~13000 per cm^{-2} and N:B ratio of 0.66 (4 h).

Video S6. Interaction of neutrophils (red) with attached *S. aureus* (green) when neutrophils were added after giving bacteria a 3 h head start (4 h).

Video S7. Computational simulation of neutrophil-bacteria interaction on a two-dimensional surface during a 4 h interval. Six bacterial colonies survive the interaction. Figure 5A illustrates the paths taken by neutrophils during this simulation.

Video S8. Computational simulation of neutrophil-bacteria interaction on a two-dimensional surface during a 4 h interval with alternative initial cell locations. This case uses parameter values identical to the simulation presented in Video S7 (initial bacteria = 12, neutrophils = 8)

except that the initial locations of both cell types are different as they have been randomly placed. In this simulation, 3 bacterial colonies survive to the end of the 4 h simulation period.

Video S9. Computational simulation of neutrophil-bacteria interaction on a two-dimensional surface during a 4 h interval with identical cell locations. This case uses parameter values and initial cell locations that are identical to the simulation presented in Video S7 to show that the paths taken by neutrophils are quite different as these are stochastic in nature.

Table S1. Random motility coefficient from mean square displacement versus time analysis. The coefficient did not vary significantly between fields of view where there were bacteria and neutrophils or where neutrophils were alone.

Condition	*n*	(cm^2 s^{-1}) D_m	(cm^2 s^{-1}) SD	Mean R^2
Neutrophils alone	4	2.15×10^{-8}	0.72×10^{-8}	0.950
Neutrophils + bacteria	4	3.17×10^{-8}	0.35×10^{-8}	0.988
All	8	2.67×10^{-8}	0.75×10^{-8}	0.969

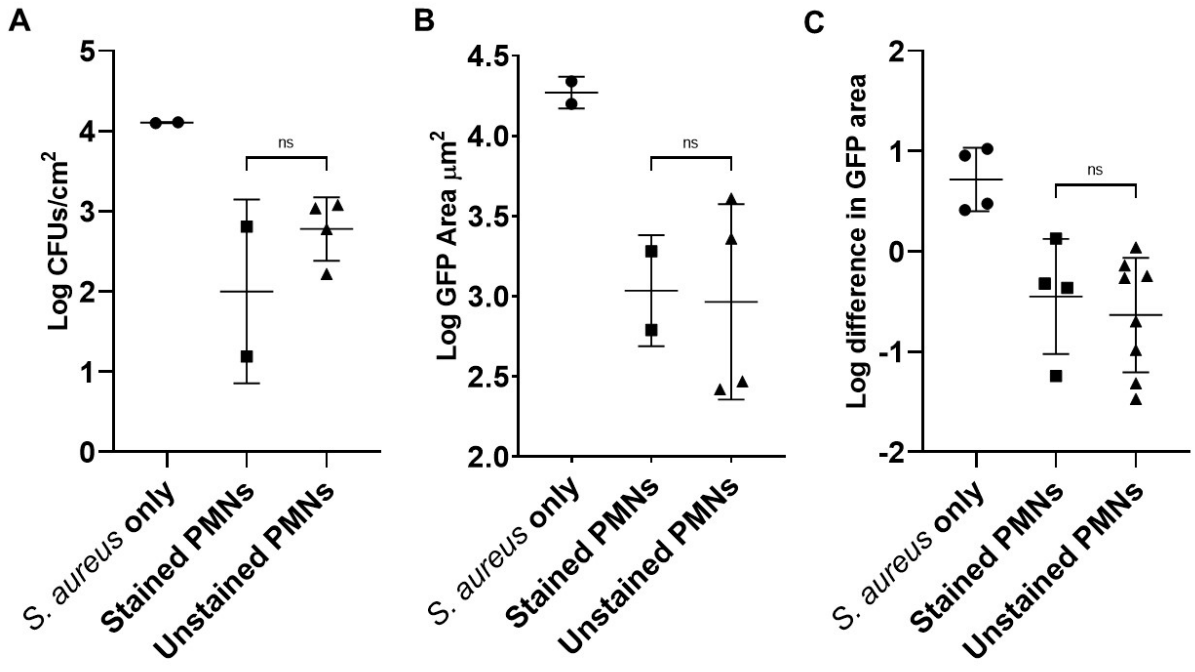

Figure S1. LysoBrite staining does not affect killing of *S. aureus* by neutrophils. Approximately 10^3 CFUs/cm^2 were attached to the surface and challenged with neutrophils that had been stained with LysoBrite or received a sham treatment. (*A*) Bacteria were scraped from the surface, vortexed, and plated on tryptic soy agar to determine remaining viable bacteria on the surface. *n* = 2 (control and stained PMNs) or 4 (unstained PMNs) from 2 independent experiments. (*B*) A stitched image of the entire well was generated using the 10x objective to determine the total amount of GFP area remaining in each well after a 4 hour challenge with neutrophils. *n* = 2 (control and stained PMNs) or 4 (unstained PMNs) from 2 independent experiments. (*C*) The log difference in GFP area over 4 hours for each field of view. *n* = 4 (control and stained PMNs) or 8 (unstained PMNs) fields of view from 2 independent experiments. Error bars represent standard deviation of the sample. Differences between stained and unstained neutrophils were not significant by an unpaired *t* test.

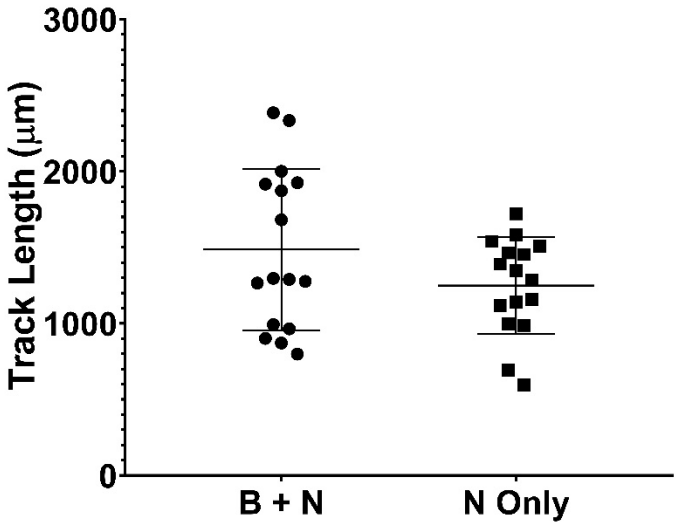

Figure S2. Neutrophil track length is similar on a sterile surface or on a surface seeded with *S. aureus*. The average speed of all neutrophils in a field of view was calculated for each frame and then integrated with respect to time to obtain an average track length value. The average distance traveled by a neutrophil did not vary between wells with bacteria and wells without bacteria ($p = 0.1368$ by an unpaired t test). $n = 16$ fields of view each from 5 independent experiments. B+N denotes bacteria with neutrophils; N only denotes neutrophils in the absence of bacteria. Error bars represent standard deviation of the sample.

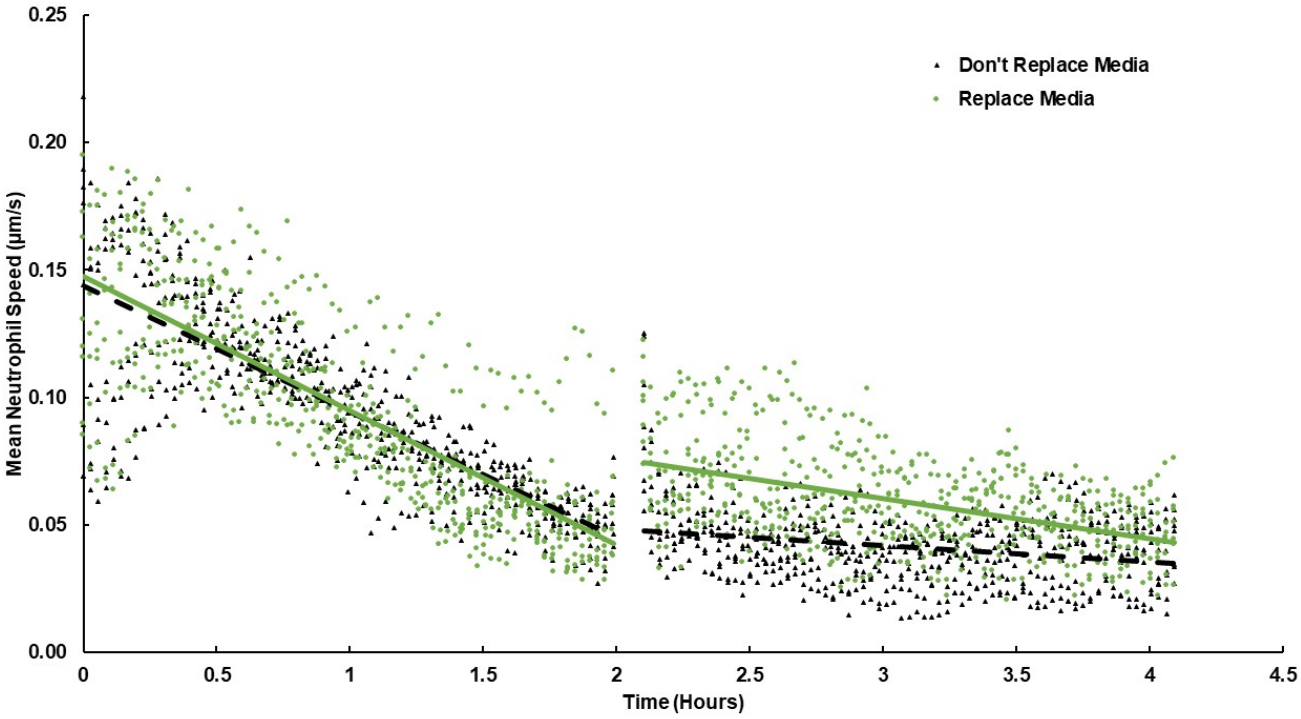

Figure S3. Mean neutrophil speed with and without medium supplementation. Experiments were performed with bacteria present. Old medium was gently removed via pipette and replaced with 10% human serum in HBSS from the same donor (serum was kept on ice and warmed to 37°C prior to addition) at 2 h. Neutrophil speed was not restored to starting levels when fresh medium was added, however a slight increase in speed was observed compared to control wells ($p < .0001$). $n = 8$ fields of view, 2 independent experiments.

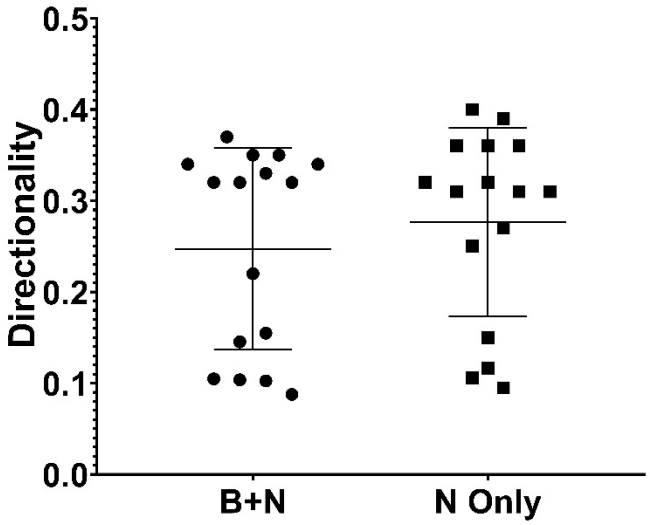

Figure S4. Neutrophil directionality measured by dividing displacement by total distance traveled. No statistically significant difference was observed between experiments with bacteria and neutrophil only controls ($p = 0.4453$ by an unpaired t test). *n* = 16 fields of view each from 5 independent experiments. B+N denotes bacteria with neutrophils; N only denotes neutrophils in the absence of bacteria. Error bars represent standard deviation of the sample.

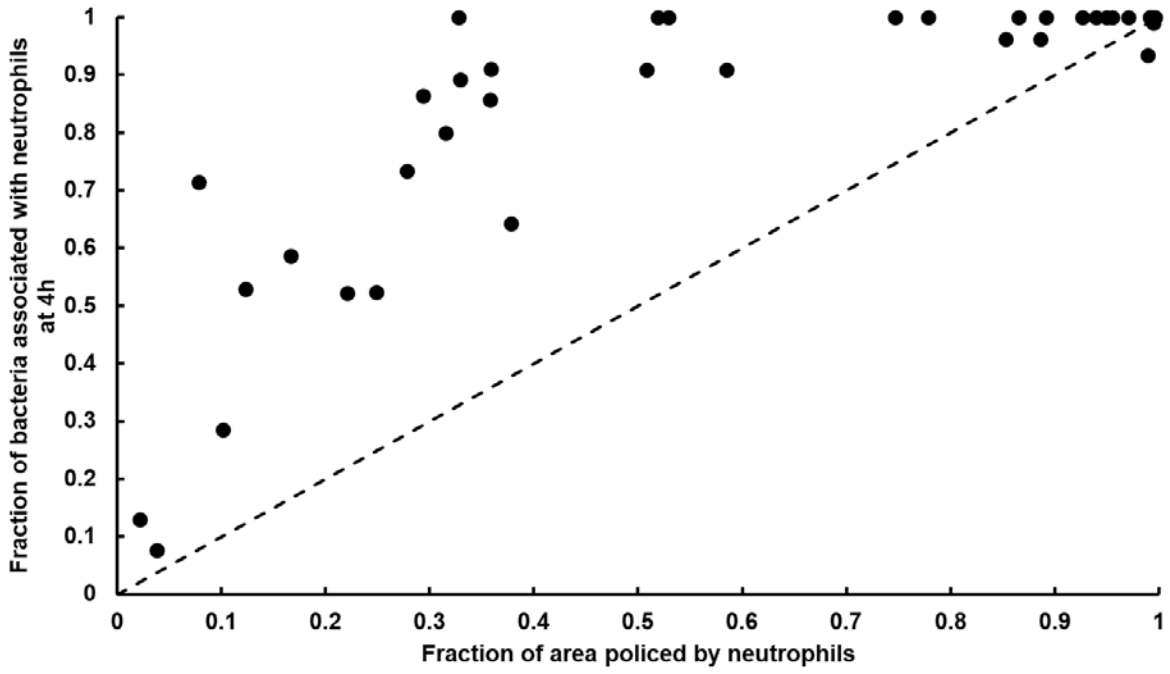

Figure S5. Fraction of bacterial objects discovered as a function of the fraction of the surface area patrolled by neutrophils. The fraction of bacterial aggregates that were discovered by a neutrophil within the 4 hour observation window were determined manually. The dashed line represents the expected curve if aggregate discovery was purely random. *n* = 39 fields of view from 9 independent experiments.

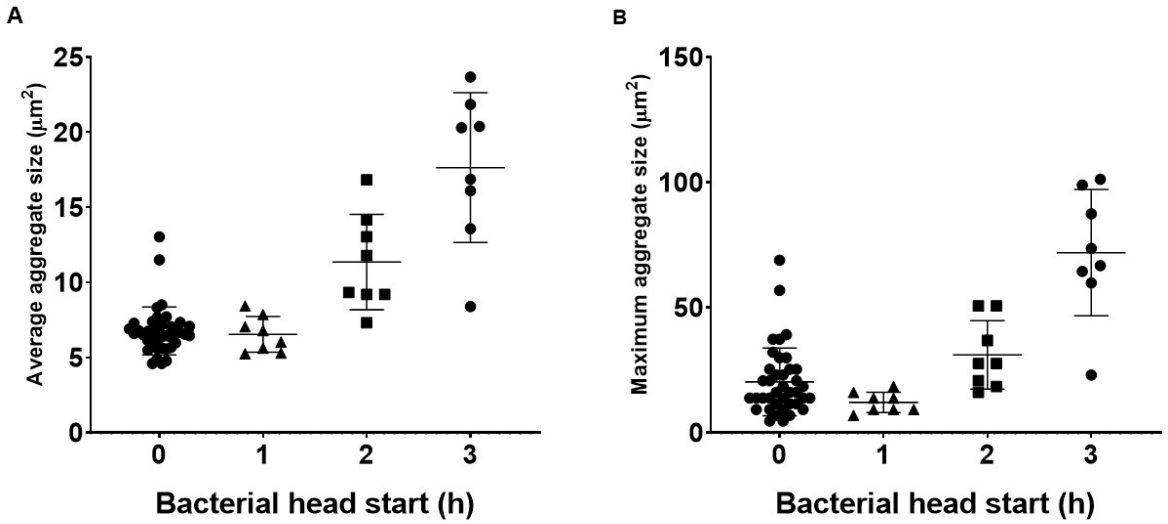

Figure S6: *S. aureus* aggregate sizes at $t = 0$. (*A*) The average size of a *S. aureus* aggregate at the start of imaging given different head start times. Each point represents the average size of all aggregates in a field of view. (*B*) The maximum observed aggregate size in a field of view at the start of imaging. $n = 24$ fields of view from 4 independent experiments for head start data. $n = 39$ fields of view from 9 independent experiments for without head starts. Error bars represent standard deviation of the sample.

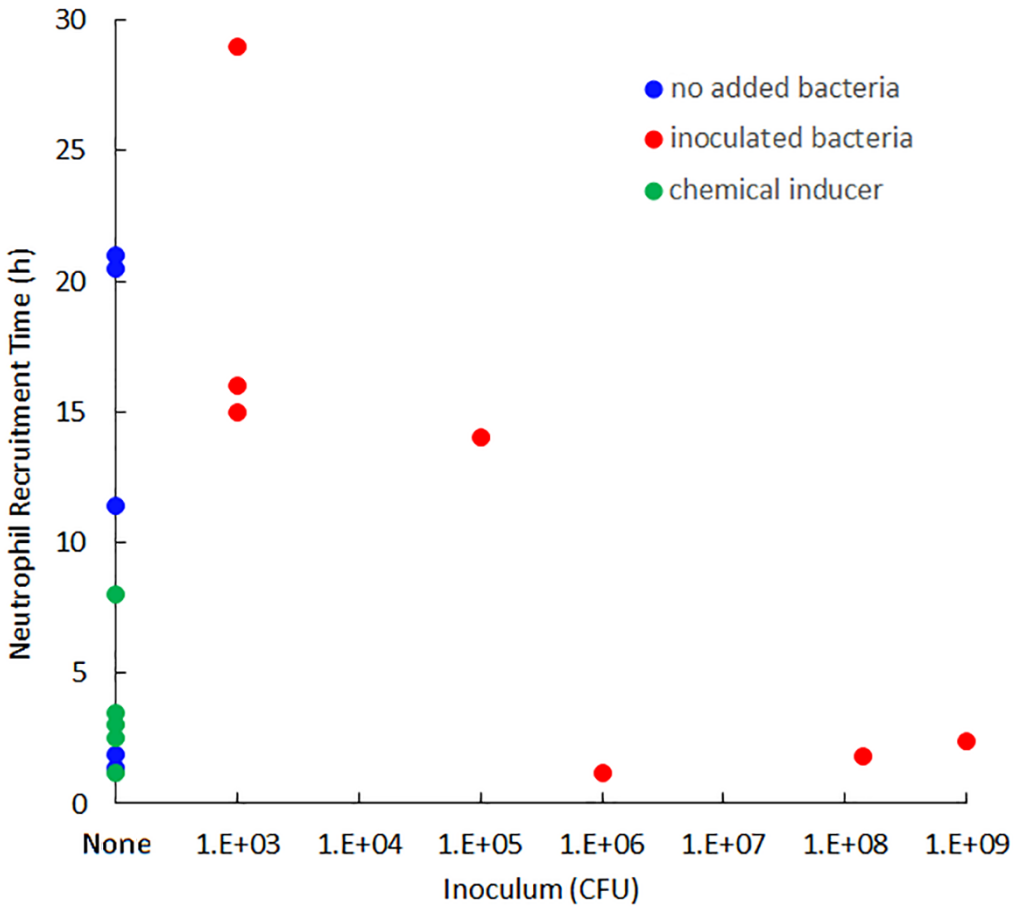

Figure S7. Neutrophil recruitment times measured in murine models. See the supplemental methods that follow for details.

Methods for literature survey of neutrophil recruitment times in murine models. We identified 18 published data sets from 14 papers (Table S2) that contained sufficient quantitative information to extract a numerical value of a characteristic neutrophil recruitment time. This time was estimated by fitting a logistic function, which is an S-shaped curve, to neutrophil signal versus time data of the form

$$N(t) = \frac{N^*}{1 + \exp\left(-k(t - t_o)\right)}$$

where $N(t)$ is neutrophil signal as a function of time, N^* is the plateau neutrophil signal at long time, t is time, k is a parameter reflecting the steepness of the response, and t_o is the characteristic time for the response to occur. The parameter t_o is the time value plotted in Figure S5. This time corresponds to the inflection point of the S-shaped curve.

The data sets analyzed are summarized in Table S2 below. The data include experiments with chemical inducers (no added bacteria), inoculated *Staphylococcus aureus* or *Staphylococcus epidermidis* (other microorganisms were excluded from the search), and some controls in which implants without added bacteria were investigated.

Table S2. Summary of neutrophils recruitment times, anatomical sites, stimuli, and sources.

		no bacteria (h)	bacteria (h)	chemical (h)	(cfu)	
Site	Stimulus	t_o	t_o	t_o	Inoculum	Source
skin on back	punch biopsy (no inoculation)	11.4			none	1
subQ	Ti disk, uninfected	20.5			none	2
subQ	Ti disk coated with *S. aureus*		21		NR	2
spine, L4 process	Stainless steel (SS) implant - control	21			none	3
spine, L4 process	SS implant inoculated with *S. epidermidis*		29		10^3	3
subQ	agar bead containing *S. aureus*		1.2		10^6	4
knee joint	SS implant, *S. aureus* strain Xen 40		16		10^3	5
knee joint	SS implant, *S. aureus* strain ALC2906		15		10^3	5
peritoneum	injection 30 μg LPS			8	none	6
knee joint	injection of *S. aureus*		14		10^5	7
pleural cavity	injection of 100 μg zymosan			3	none	8
air pouch on back	injection of 0.5 μg MIP-2			1.2	none	9
peritoneum	injection of 1 mg zymosan			3.5	none	10
liver	sterile thermal injury	1.9			none	11
skin on back	6 mm full thickness punch biopsy	1.4			none	12
peritoneum	injection of 5 mg/kg peptidoglycan			2.5	none	13
peritoneum	injection of *S. aureus*		2.4		10^9	13
peritoneum	injection of *S. aureus*		1.8		$1.4x10^8$	14
	Mean	11.2	12.6	3.6		
	SD	9.6	10.1	2.6		

NR – not reported; SD – standard deviation.

References

1. Kim MH, Liu W, Borjesson DL, Curry FR, Miller LS, Cheung AL, Liu FT, Isseroff RR, Simon SI. 2008. Dynamics of neutrophil infiltration during cutaneous wound healing and infection using fluorescence imaging. J Invest Dermatol 128:1812-1820.

2. Stavrakis AI, Niska JA, Shahbazian JH, Loftin AH, Ramos RI, Billi F, Francis KP, Otto M, Bernthal NM, Uslan DZ, Miller LS. 2014. Combination prophylactic therapy with rifampin increases efficacy against an experimental *Staphylococcus epidermidis* subcutaneous implant-related infection. Antimicrob Agents Chemother 58:2377-2386.

3. Dworsky EM, Hegde V, Loftin AH, Richman S, Hu Y, Lord E, Francis KP, Miller LS, Wang JC, Scaduto A, Bernthal NM. 2017. Novel in vivo mouse model of implant related spine infection. J Orthop Res 35:193-199.

4. Harding MG, Zhang K, Conly J, Kubes P. 2014. Neutrophil crawling in capillaries; a novel immune response to *Staphylococcus aureus*. PLoS Pathog 10:e1004379.

5. Pribaz JR, Bernthal NM, Billi F, Cho JS, Ramos RI, Guo Y, Cheung AL, Francis KP, Miller LS. 2012. Mouse model of chronic post-arthroplasty infection: noninvasive in vivo bioluminescence imaging to monitor bacterial burden for long-term study. J Orthop Res 30:335-340.

6. Gonçalves AS, Appelberg R. 2002. The involvement of the chemokine receptor CXCR2 in neutrophil recruitment in LPS-induced inflammation and in *Mycobacterium avium* infection. Scand J Immunol 55:585-591.

7. Boff D, Oliveira VLS, Queiroz Junior CM, Silva TA, Allegretti M, Verri WA Jr, Proost P, Teixeira MM, Amaral FA. 2018. CXCR2 is critical for bacterial control and development of joint damage and pain in *Staphylococcus aureus*-induced septic arthritis in mouse. Eur J Immunol 48:454-463.

8. Takeshita K, Sakai K, Bacon KB, Gantner F. 2003. Critical role of histamine H4 receptor in leukotriene B4 production and mast cell-dependent neutrophil recruitment induced by zymosan in vivo. J Pharmacol Exp Ther 307:1072-1078.

9. McColl SR, Clark-Lewis I. 1999. Inhibition of murine neutrophil recruitment in vivo by CXC chemokine receptor antagonists. J Immunol 163:2829-2835.

10. Watzlawick R, Kenngott EE, Liu FD, Schwab JM, Hamann A. 2015. Anti-inflammatory effects of IL-27 in zymosan-induced peritonitis: inhibition of neutrophil recruitment partially explained by impaired mobilization from bone marrow and reduced chemokine levels. PLoS One 10:e0137651.

11. McDonald B, Pittman K, Menezes GB, Hirota SA, Slaba I, Waterhouse CC, Beck PL, Muruve DA, Kubes P. 2010. Intravascular danger signals guide neutrophils to sites of sterile inflammation. Science 330:362-366.

12. Liu M, Chen K, Yoshimura T, Liu Y, Gong W, Le Y, Gao JL, Zhao J, Wang JM, Wang A. 2014. Formylpeptide receptors mediate rapid neutrophil mobilization to accelerate wound healing. PLoS One 9:e90613.

13. Mullaly SC, Kubes P. 2006. The role of TLR2 in vivo following challenge with *Staphylococcus aureus* and prototypic ligands. J Immunol 177:8154-8163.

14. Weiss E, Hanzelmann D, Fehlhaber B, Klos A, von Loewenich FD, Liese J, Peschel A, Kretschmer D. 2018. Formyl-peptide receptor 2 governs leukocyte influx in local *Staphylococcus aureus* infections. FASEB J 32:26-36.

Supplemental Material: Solution of the Chemoattractant Concentration Equation. The chemoattractant concentration $u(\mathbf{x}, t)$ satisfies the equation

$$u_t = D_1 \nabla^2 u + 2\beta \sum_{j=1}^{12} \sum_{k,\ell \in \mathbb{Z}} c_j(t)\, \delta(\mathbf{x} - (\mathbf{x_j} + (800k, 800\ell, 0))),$$

with initial and boundary conditions

$$u(\mathbf{x}, 0) = 2\beta \sum_{j=1}^{12} \sum_{k,\ell \in \mathbb{Z}} \delta(\mathbf{x} - (\mathbf{x_j} + (800k, 800\ell, 0))), \quad \frac{\partial u}{\partial z}(x, y, 0, t) = 0.$$

Here,

$$c_j(t) = \begin{cases} e^{rt} & 0 \leqslant t < T_j \\ 0 & t \geqslant T_j \end{cases}$$

is the population of colony j, and T_j is the time of first encounter of a neutrophil with that colony (T_j may be larger than the total run time of 240 min.).

Note by linearity that we can decompose

$$u(\mathbf{x}, t) = \sum_{j=1}^{12} u_j(\mathbf{x}, t)$$

where u_j is the contribution to total chemoattractant concentration from bacteria colony j, where u_j satisfies

$$(u_j)_t = D_1 \nabla^2 u_j + 2\beta \sum_{k,\ell \in \mathbb{Z}} c_j(t)\, \delta(\mathbf{x} - (\mathbf{x_j} + (800k, 800\ell, 0))),$$

with initial and boundary conditions

$$u_j(\mathbf{x}, 0) = 2\beta \sum_{k,\ell \in \mathbb{Z}} \delta(\mathbf{x} - (\mathbf{x_j} + (800k, 800\ell, 0))), \quad \frac{\partial u_j}{\partial z}(x, y, 0, t) = 0.$$

For $t < T_j$ these systems have solutions

$$\begin{aligned} u_j(\mathbf{x}, t) &= \sum_{k,l \in \mathbb{Z}} \int_0^t \frac{2\beta c_j(\hat{t}\,)}{(4\pi D_1 (t - \hat{t}\,))^{3/2}} \exp\left(-\frac{|\mathbf{x} - (\mathbf{x_j} + (800k, 800\ell, 0))|^2}{4D_1(t - \hat{t}\,)} \right) d\hat{t} \\ &= \sum_{k,\ell \in \mathbb{Z}} \frac{\beta c_j(t)}{4\pi D_1 |\mathbf{x} - (\mathbf{x_j} + (800k, 800\ell, 0))|} \\ &\quad \left[\exp\left(-|\mathbf{x} - (\mathbf{x_j} + (800k, 800\ell, 0))| \sqrt{\frac{r}{D_1}} \right) \operatorname{erfc}\left(\frac{|\mathbf{x} - (\mathbf{x_j} + (800k, 800\ell, 0))|}{\sqrt{4D_1 t}} - \sqrt{rt} \right) \right. \\ &\quad \left. + \exp\left(|\mathbf{x} - (\mathbf{x_j} + (800k, 800\ell, 0))| \sqrt{\frac{r}{D_1}} \right) \operatorname{erfc}\left(\frac{|\mathbf{x} - (\mathbf{x_j} + (800k, 800\ell, 0))|}{\sqrt{4D_1 t}} + \sqrt{rt} \right) \right], \end{aligned}$$

where $\operatorname{erfc}(z) = 1 - \operatorname{erf}(z) = \frac{2}{\sqrt{\pi}} \int_z^\infty e^{-t^2} dt$ is the complementary error function.

For $t \geqslant T_j$, the solution is

$$
\begin{aligned}
u_j(\mathbf{x}, t) \; &= \sum_{k,\ell \in \mathbb{Z}} \int_0^{T_j} \frac{2\beta c_j(\hat{t}\,)}{(4\pi D_1 (t - \hat{t}\,))^{3/2}} \exp\left(\frac{-|\mathbf{x} - (\mathbf{x_j} + (800k, 800\ell, 0))|^2}{4D_1(t - \hat{t}\,)} \right) d\hat{t} \\
&= \sum_{k,\ell \in \mathbb{Z}} \frac{\beta c_j(t)}{4\pi D_1 |\mathbf{x} - (\mathbf{x_j} + (800k, 800\ell, 0))|} \\
&\left\{ \exp\left(-|\mathbf{x} - (\mathbf{x_j} + (800k, 800\ell, 0))| \sqrt{\frac{r}{D_1}} \right) \right. \\
&\left[\operatorname{erfc}\left(\frac{|\mathbf{x} - (\mathbf{x_j} + (800k, 800\ell, 0))|}{\sqrt{4D_1 t}} - \sqrt{rt} \right) - \operatorname{erfc}\left(\frac{|\mathbf{x} - (\mathbf{x_j} + (800k, 800\ell, 0))|}{\sqrt{4D_1 (t - T_j)}} - \sqrt{r(t - T_j)} \right) \right] \\
&+ \exp\left(|\mathbf{x} - (\mathbf{x_j} + (800k, 800\ell, 0))| \sqrt{\frac{r}{D_1}} \right) \\
&\left. \left[\operatorname{erfc}\left(\frac{|\mathbf{x} - (\mathbf{x_j} + (800k.800\ell, 0))|}{\sqrt{4D_1 t}} + \sqrt{rt} \right) - \operatorname{erfc}\left(\frac{|\mathbf{x} - (\mathbf{x_j} + (800k, 800\ell, 0))|}{\sqrt{4D_1 (t - T_j)}} + \sqrt{r(t - T_j)} \right) \right] \right\}
\end{aligned}
$$